https://dx.doi.org/10.1016/j.tws.2018.04.006

Axial compressive strength of welded S460 steel columns at elevated temperatures

Han Fang[a] and Tak-Ming Chan[a,*]

Department of Civil and Environmental Engineering, The Hong Kong Polytechnic University, Hung Hom, Hong Kong, China

Abstract

This paper presents an investigation on the structural performance of welded S460 steel columns under axial compression at elevated temperatures using finite element analysis. Stub and long columns with box and H- sections were considered. A new stress-strain curve model for S460 steel at elevated temperatures was proposed and adopted to obtain the stress-strain curves for the finite element analysis. A finite element model was developed and verified against the available test data for welded S460 steel columns subject to axial compression at room and elevated temperatures. A parametric study was carried out to generate additional data of the axial compressive strength of box and H-section columns with various cross-section slenderness and column slenderness ratios at elevated temperatures. The obtained numerical results of the column strength were compared with the design predictions using the European and American specifications and the direct strength method by substituting the material properties at elevated temperatures. It was found that the provisions in European and American standards for elevated temperature conditions provide relatively conservative predictions. The direct strength method overestimates the strength of stub columns while accurately predicts the strength of long columns at elevated temperatures. Modifications are proposed for the European and American standards and direct strength method and these modified design rules are recommended to be used to more accurately estimate the design strength for welded S460 steel columns at elevated temperatures.

Keywords: Welded H- and box section columns, axial compression, elevated temperatures, finite element analysis, design, S460 steel

1. Introduction

The use of high strength steel (HSS) with nominal yield strength over 460MPa in structural construction brings about considerable advantages over mild steel. By using HSS, lighter structural

members with smaller cross-section sizes can be adopted, resulting in the significant material savings and easer handling during construction. Consequently, the transportation and construction costs can be reduced. Besides, the lesser consumption of steel materials also generates higher environmental efficiency. In order to carry out accurate design of HSS structures, extensive research studies have been conducted to determine the behaviour of cold-formed and welded HSS columns under compression at room temperature. The local buckling behaviour and strength of HSS stub columns were investigated in experiments and numerical modelling [1-6] and revised slenderness limits for cross-section classification were proposed [7]. The global buckling resistance of HSS columns was also investigated [4-5, 8-11] and suitable buckling curves for the design of HSS columns were also proposed [8-10, 12]. However, although great progress in developing room temperature design guidance for HSS columns has been made, the performance of HSS columns under elevated temperature conditions has received much less attention and needs to be thoroughly investigated for designing the structures for the possibility of fire exposure.

The behaviour of BISALLOY 80 high strength steel (with the nominal yield strength of 690 MPa) columns with box and I- sections at elevated temperatures was investigated numerically by Chen and Young [13]. A parametric analysis was performed to determine the temperature effect on the strength of both stub columns with various cross-section slenderness and long columns with different slenderness ratios. The suitability of specifications in European, American and Australian standards and direct strength method [17] for BISALLOY 80 high strength steel columns at elevated temperatures was assessed by comparing the results of the parametric study with those of the column strength predicted based on the standards with the substitution of material properties at elevated temperatures. It was found that European and American specifications and direct strength method could be used to conservatively predict the strength of BISALLOY 80 high strength steel columns at elevated temperatures. Wang and co-workers [19] conducted experiments to investigate the axial compressive strength of welded Q460 steel columns at only two temperatures of 450^{o}C and 650^{o}C and the column specimens with two cross-section sizes were tested. It was found that the axial compressive strength of the columns at 650^{o}C was significantly lower than that of the columns at 450^{o}C due to the deterioration of material strength and stiffness with increasing temperatures. However, no systematic study has been conducted to investigate the strength of 460MPa steel columns at varying elevated temperatures that the structures may experience under fire condition.

In this study, the axial compressive strength of welded S460 steel columns with box and H- sections at elevated temperatures was investigated using finite element analysis. Firstly, a stress-strain model for S460 steel at elevated temperatures was proposed based on the experimental results obtained by Qiang and the co-workers [20] for structural design and analysis. Secondly, a finite element model was initially developed and validated against the test results of the welded S460 steel columns at room

and elevated temperature conditions [1, 8-9, 19, 21]. Upon validation of the finite element model, a parametric study was subsequently carried out to determine the strength of welded S460 steel columns with various cross-sectional slenderness and column slenderness ratios at a wide range of elevated temperatures. Finally, the results of finite element analysis were compared with the design strength predictions obtained based on the provisions in European standard [14], American standard [15] and the direct strength method (DSM). Modifications to the European and American standards and DSM are suggested in order to obtain more accurate and safe predictions of the column strength for structural design.

2. Proposed stress-strain curve model

2.1 Stress-strain curve model proposed by other researchers

A stress-strain curve model is given in EN1993-1-2 [14] for temperatures up to 1200^{o}C and is based on test results on hot-rolled normal strength steel. Schneider and Lange [21] have found that the stress-strain curves for S460 steel predicted using the model in EN1993-1-2 are very different from the curves obtained in experiments. Stress-strain curve models for elevated temperatures were also developed based on the Ramberg–Osgood equation [23] for hot-rolled steel [24], S420 steel [25] and light gauge steel [26]. In these models, the basic form of the Ramberg–Osgood equation for elevated temperatures is given as

$$\varepsilon_T = \frac{f_T}{E_T} + \beta \left(\frac{f_{y,T}}{E_T}\right)\left(\frac{f_T}{f_{y,T}}\right)^n \quad (1)$$

where ε_T is the strain at temperature T ^{o}C, f_T is the stress at temperature T ^{o}C, $f_{y,T}$ is the yield stress at temperature T ^{o}C, E_T is the elastic modulus at temperature T ^{o}C. For the coefficients of β and n, different studies provided different values and calculation methods. The stress–strain curves for S460 were predicted using these stress–strain curve models [24-26]. These predicted curves were compared with the curves obtained in experiments which were conducted by Qiang and co-workers [20], as shown in Figs. 1-3 respectively. As can be seen in the figures, the differences between the stress-strain curves predicted using the three proposed models and those from the test results are quite significant. Therefore, using the predicted curves from these models can lead to inaccurate structural analysis and design. An accurate model for S460 steel at elevated temperatures is needed.

2.2 New stress-strain curve model

The prediction of stress-strain curves based on Eq. (1) compares reasonably with the experimental stress-strain relationship in the elastic stage when the stress increases linearly with the increment of strain. However, Eq. (1) provides inaccurate simulation of the stress-strain relationship in the inelastic

stage when the stress becomes higher than the proportional limit of the material, as observed in Figs. 1-3. This is mainly due to the variation of n, as a parameter related to the strain hardening in the inelastic stage, with the increment of strains [16, 27]. Thus, using a constant value of n for predicting the stress with increasing strain in both elastic and inelastic stages leads to inaccurate stress-strain curves.

A new two-phase stress-strain model is proposed in this study in order to accurately estimate the stress-strain curves of the S460 steel at temperatures from room temperature (approximately 22^{o}C) to 700^{o}C. This model (Eqs. (2)-(4)) was obtained based on the stress–strain curve model proposed by Mirambell and Real [27] for stainless steel at room temperature.

$$\varepsilon_T = \begin{cases} \frac{f_T}{E_T} + 0.002\left(\frac{f_T}{f_{0.2,T}}\right)^{n_0}, \ for\ f_T \le f_{0.2,T} \\ \frac{f_T - f_{0.2,T}}{E_T} + \varepsilon_{u,T}\left(\frac{f_T - f_{0.2,T}}{f_{u,T} - f_{0.2,T}}\right)^{n_1} + \varepsilon_{0.2,T}, \ for f_T \le f_{0.2,T} \end{cases} \quad (2)$$

$$n_0 = 12 - \mathrm{T}/100 \quad (3)$$

$$n_1 = 2.1 - 3\mathrm{T}/1000 \quad (4)$$

Here, $f_{0.2,T}$ is the 0.2% proof stress at temperature T ^{o}C, $\varepsilon_{u,T}$ is the ultimate strain at temperature T ^{o}C, $f_{u,T}$ is the ultimate strength at temperature T ^{o}C, $\varepsilon_{0.2,T}$ is the strain corresponding to the $f_{0.2,T}$ at temperature T ^{o}C and T is the temperature value in degree Celsius (^{o}C). Eqs. (2)-(4) were applied to obtain the stress-strain curves of S460 steel at elevated temperatures. Each of the $f_{0.2,y}$, $\varepsilon_{u,T}$, $f_{u,T}$, E_T and $\varepsilon_{0.2,T}$ parameters in Eq.(2) was determined by multiplying the value of the parameter at room temperature with the reduction factors which were obtained for the material at elevated temperatures through experimental investigations conducted by Qiang et al. [20]. The obtained stress-strain curves were plotted together with the experimental results [20] for comparison, as shown in Fig. 4. As can be seen in the figure, the stress-strain curves obtained using the proposed model closely match those obtained in experiments. Therefore, the proposed new stress-strain model can be applied to accurately predict the stress-strain curves of S460 at elevated temperatures for structural design and analysis.

3. Finite element model

A finite element model using the software package ABAQUS [28] was developed to simulate the tests on welded S460 steel stub and long columns under concentric compression at room and elevated temperatures [1, 8-9, 19, 21]. The key characteristics of the finite element model and validation of the model against the column test results are presented in this section. A parametric study to further

investigate the strength of welded S460 steel columns at various elevated temperatures was conducted using the validated model, as presented in Section 4.

3.1 Element type and material modelling

The welded S460 columns were modelled using the four-node shell element S4R with reduced integration. The S4R element has six degrees of freedom per node. This type of element has been shown to be suitable for obtaining accurate finite element analysis results in similar studies [4, 13]. A mesh convergence study was conducted and the mesh size of 20mm*20mm was found to be suitable and adopted for all models. Even when a finer mesh size of 10mm*10mm was used, the change in the finite element analysis results for columns was only 0.23% on average. The stress-strain relationship of the material was reproduced using the multi-linear stress-strain curve model in ABAQUS. The stress-strain curves of S460 steel at different temperatures were first obtained using the proposed model presented in section 2.2, and subsequently converted into the true stress and logarithmic plastic true strain curves which were incorporated into the finite element analysis.

3.2 Boundary conditions and load application

The boundary conditions of the ends of the columns were modelled according to the set-up of the column tests. The stub column specimens tested at room temperature [1] and the columns tested at elevated temperatures [19] had fixed ends. The long column specimens tested at room temperature [8-9, 21] were pin-supported. In order to simulate these boundary conditions, two reference points were coupled with the nodes of both end surfaces of each column. For the columns with fixed ends, the reference points of each column were fixed against all degrees of freedom except for the displacement at the loaded end in the direction of the applied load. As for each pin-supported column with box section, the reference points were restrained against all degrees of freedom except for the rotations about the axis of buckling at both ends and the displacement in the direction of the applied load at the loaded end. The boundary conditions applied for the pin-supported columns with H-section were the same as those of the box-section columns except that the rotations about the major axis at both ends of each column were also restrained. The load was applied at the reference point of the loaded end of each column by specifying an axial displacement in a RIKS step in ABAQUS. The modified RIKS method was employed in this study to estimate the load-displacement response of the columns including the post-ultimate behaviour.

3.3 Geometric imperfection and residual stress

Initial geometric imperfection of the column structures was accounted for in the finite element analysis. The geometric imperfection was incorporated into the load-displacement analysis of each

column structure in the form of the lowest elastic buckling mode shape obtained by conducting a prior elastic eigenvalue analysis, with the amplitude given in those experimental studies of the column structures. The local imperfection amplitudes given in [1] for stub columns tested at room temperature and those provided in [19] for columns tested at elevated temperatures respectively were included in the analysis. Global imperfections were found in the long columns tested at room temperature and the measured amplitudes presented in [8-9, 21] were incorporated into the analysis of the columns. Since no local imperfections of the long columns were provided [8-9, 21], the amplitudes of local imperfections suggested by Shi et al. [1] for welded S460 box and H-section columns were used in the finite element analysis for the columns. Thus, the local imperfection amplitude was taken as 0.5% of the element height for any plate element of box section and the web of H-section long columns. For the flange of the H-section long columns, the local imperfection amplitude was taken as 1% of the width of the flange.

Residual stresses in welded S460 steel box and H-sections were measured at room temperature by Wang and the co-workers [29-30]. The magnitudes and pattern of residual stresses obtained based on the proposed residual stress models in these studies were included as initial stresses in the analysis of columns under the room temperature condition. Residual stresses in welded steel structures subject to elevated temperatures were investigated by Dong et al. [32] and were found to decrease significantly with increasing temperatures. Due to this release of residual stresses, the influence of residual stresses on the column behaviour at elevated temperatures has been suggested to be very limited [33-35]. Thus, the residual stresses were neglected for the analysis of columns subject to elevated temperatures.

3.4 Validation of the finite element model

The finite element model was validated against 18 test results of welded S460 stub and long columns at room [1, 8-9, 21] and elevated temperatures [19]. The 18 columns for modelling are presented in Table 1. The column labels in the table are developed based on the cross-sectional shape and nominal dimensions. For example, the label “B110*110*11L3320” defines the following specimen: “B” indicates the box section column; the digits following letter “B” represent the nominal width, height and thickness of the cross-section; the letter “L” indicates the length of the column, and the following digits represent the length of the column in millimetres (3320mm). The label “H160*170*21*11L3304” defines an H-section indicated by the letter, “H”; the following digits represent the nominal flange width, cross-sectional height, thickness of the flange and thickness of the web; the letter “L” indicates the length of the column followed by the column length in millimetres (3304mm). The temperatures were also given in the labels for the welded S460 columns tested at elevated temperatures. The geometry and material properties measured for these columns in the experimental investigations were used in the analysis.

The finite element analysis (FEA) results of ultimate compressive strength of the columns were compared with those experimental results, as shown in Table 1. It shows in the table that the ultimate compressive strength of the columns was accurately estimated using the finite element model. The analysis results of the load-displacement responses of the columns also agreed well with those from experiments, as shown in Fig. 5 for the load-deflection curves of box section stub and long columns under room temperature condition and in Fig. 6 for the load-end shortening curves for columns subject to elevated temperatures. Furthermore, the failure modes of the columns, including flexural buckling (F) and local buckling (L), were also accurately predicted in the analysis, as shown in Table 1. The deformation of the columns with the flexural and local buckling failures is also presented in Fig. 7 for box section stub and long columns at room temperature and H-section columns at room and elevated temperatures. Based on all these results, it can be concluded that the finite element model is validated to accurately predict the ultimate compressive strength, load-displacement behaviour and failure modes of welded S460 box and H-section columns at room and elevated temperatures.

4. Parametric study

Having the finite element model validated, a parametric study was conducted to thoroughly investigate the influence of temperature on the compressive strength of welded S460 steel box and H-section columns with various cross-sectional slenderness and column slenderness ratios. The cross-section sizes of columns investigated was based on the column cross-sections investigated experimentally [1, 8-9, 21]. Both fixed-ended stub columns and pin-supported long columns were investigated. Nine different temperatures of 22 (room temperature), 300, 400, 450, 500, 550, 650 and 700^{o}C were considered. Various cross-sectional slenderness for stub columns was achieved by varying the cross-sectional thickness or width and height of the sections. For box section stub columns, the width-to-thickness ratios (b/t) range from 13 to 48. For H-section stub columns, the width-to-thickness ratios (b/t) range from 6.9 to 24 for the flanges, whereas the width-to-thickness ratios (h/t) range from 20.1 to 72.6 for webs. The dimensions for the stub columns are provided in Table 2. The section classification of the stub columns at room temperature was also estimated based on the European standard [31] and is presented in Table 2. A range of column slenderness ratios (L/r) between 38 and 100 was also achieved by varying the column lengths in the analysis of long columns. The non-dimensional slenderness ratio ($\bar{\lambda}$) of the long columns under room temperature condition was also calculated according to the European standard [31]. The dimensions and slenderness ratios for the long columns are provided in Table 3.

The material properties used for the parametric study was obtained using the proposed stress-strain curve model (Eqs. (2)-(4)) based on the measured material properties at room temperature [1, 8-9, 21] and the reduction factors given in [20] for the material properties at elevated temperatures. These

reduction factors for elastic modulus (E_T), 0.2% proof stress ($f_{0.2}$), stress at 2% strain ($f_{2.0,T}$), ultimate strength ($f_{u,T}$) and the ultimate strain (ε_u) at different temperatures are provided in Table 4. The local geometric imperfection incorporated into the modelling of both stub and long columns was based on the amplitudes per unit sectional width and height for box and H-sections respectively [1], as introduced in section 3.3. These amplitudes of local geometric imperfections together with the global geometric imperfections were also found to provide accurate FEA results for long columns, as illustrated in section 3.4. The global imperfection incorporated into the modelling of pin-supported long columns was estimated based on the measured global imperfection amplitudes per unit column length [8-9, 21]. Residual stresses were taken into account for the columns under room temperature condition according to the arrangement introduced in section 3.3. At elevated temperatures of 300 and 400^{o}C, the strength of welded steel columns is insensitive to residual stresses based on the investigations performed by Heidarpour et al. [36]. Besides, the FEA results for columns at elevated temperatures of 450 and 650^{o}C were obtained without considering the effect of residual stress and were in a good agreement with the column test results, as discussed in section 3.4. Thus, residual stresses were not included in the analysis for columns subject to elevated temperatures from 300 to 700^{o}C.

Based on the parametric study results, the ratios of ultimate compressive strength at temperature T ($P_{ult,T}$) to that at room temperature ($P_{ult,n}$) were plotted against temperatures for the B240*240L300 and H350*450L600 stub columns with various cross-sectional slenderness, as presented in Figs. 8(a) and (b) respectively. As shown in the figures, the temperature is a more dominant factor on the reduction rate of ultimate strength of the stub columns than the cross-sectional slenderness. The strength of box and H-section stub columns decreased gradually with increasing temperature from room temperature to 450^{o}C. At 450^{o}C, the strength of the columns was at least 80% of their strength at room temperature. With temperatures increasing from 450^{o}C to 700^{o}C, the strength of the columns reduced significantly to about 20% of the strength of the columns at room temperatures. It can also be observed in the figure that the proportion of column strength reduction for the columns with non-slender cross sections at any temperature was insensitive to the cross-sectional slenderness. The curve of $P_{ult,T}$/ $P_{ult,n}$ with temperatures for B240*240*16 column about coincides with the curve for B240*240*12 column while the curve of $P_{ult,T}$/ $P_{ult,n}$ with temperatures for H350*450*24*20 column about coincides with the curve for H350*450*20*18 column. As for the columns with slender cross sections, the column with a higher width-to-thickness ratio experienced a slightly larger proportion of column strength reduction at any elevated temperature, as shown in Fig. 8. These results would be expected because the strength of stub columns with non-slender cross sections is primarily controlled by the material strength while the strength of stub columns with slender cross sections is dependent on both material strength and stiffness [33-34]. The material strength degrades at a slower rate with

increasing temperatures than the material stiffness [20]. Thus, a higher proportion of strength reduction at elevated temperatures occurred for the stub columns with slender cross sections.

For the box and H-section long columns, the ratios of ultimate compressive strength at temperature T ($P_{ult,T}$) to that at room temperature ($P_{ult,n}$) were also plotted against temperatures, as presented in Figs. 9 (a) and (b) for B110*110*11 and H160*170*21*11 columns respectively. As can be seen in the figures, the reduction of column strength with increasing temperatures is dependent on the column slenderness ratios. Compared with the compressive strength at room temperature, the proportion of strength reduction of any box-section column with a lower slenderness ratio was lower than that of the column with a higher slenderness ratio at elevated temperatures, as shown in Fig. 9(a). As for the H-section columns, the proportion of strength reduction increased with increasing slenderness ratios up to 80 at each elevated temperature. The difference between the strength reduction rate of columns with slenderness ratios of 80 and 100 at elevated temperatures was insignificant. The different rates of strength deterioration for columns with varying slenderness ratios was obtained because the strength of columns becomes more dependent on the degradation of material stiffness than the degradation of material strength with increasing slenderness ratios of the columns [33-34]. The material strength degrades at a slower rate with increasing temperatures than the material stiffness [20]. Thus, a higher proportion of strength reduction at elevated temperatures occurred for the columns with larger slenderness ratios.

5. Design rules

5.1 Comparison with existing design rules

The FEA results of the compressive strength of the stub and long columns from the parametric study were compared with the unfactored design strength predicted using the design rules provided by EN1993-1-2 [14] and ANSI/AISC 360-16 [15] for columns subject to elevated temperatures. In addition, the direct strength method (DSM) proposed for cold-formed steel columns at room temperature [17-18] was also used to estimate the strength of the columns investigated in the parametric study and its applicability for welded S460 steel columns at elevated temperatures was also examined. In the comparisons, the geometric and material properties used for the parametric study was employed to obtain the strength of the columns based on the design standards and DSM. According to the European standard [14], the stress ($f_{2.0,T}$) at 2% strain at temperature T was used as the yield stress ($f_{y,T}$) for the design of structural members with Class 1-3 cross-sections while the 0.2% proof stress ($f_{0.2,T}$) at temperature T was used as the yield stress ($f_{y,T}$) for the design of structural members with Class 4 cross-sections. The same principle was used in estimating the design strength

based on AISC standard and DSM in order to directly compare the design strength predictions provided by the three design rules.

5.1.1 European standard

The design strength (P_{EC}) was estimated based on the Eurocode 3: Part 2 [14] which provides the design rules for compression members subject to elevated temperatures. The cross-section classification can be determined based on a reduced value for ε as

$$\varepsilon = 0.85 * \sqrt{235/f_{y,20}} \quad (5)$$

where $f_{y,20}$ is the yield strength at room temperature. The column strength, $P_{EC,}$ can be estimated based on the reduction factor (χ_{fi}) for flexural buckling. A single buckling curve proposed by Franssen and the co-workers [37] using Eqs. (6)-(9) was adopted for χ_{fi} under elevated temperature conditions in European Standard.

$$\chi_{fi} = \frac{1}{\varphi_T + \sqrt{\varphi_T^2 - \bar{\lambda}_T^2}} \quad (6)$$

$$\varphi_T = 0.5 * (1 + \alpha\bar{\lambda}_T + \bar{\lambda}_T^2) \quad (7)$$

$$\bar{\lambda}_T = \bar{\lambda} * \left(k_{y,T}/k_{E,T}\right)^{0.5} \quad (8)$$

$$\alpha = \beta * \sqrt{235/f_{y,20}} \quad (9)$$

In these equations, φ_T is the value to determine the reduction factor χ_{fi} at temperature T, $\bar{\lambda}_T$ is the non-dimensional slenderness for temperature T, $\bar{\lambda}$ is the non-dimensional slenderness at room temperature, $k_{y,T}$ is the reduction factor for yield strength at temperature T, $k_{E,T}$ is the reduction factor for elastic modulus at temperature T, α is the imperfection factor and β is the severity factor. The value of β is given as 0.65 [14, 37].

The calculated P_{EC} was compared with the strength of columns obtained in the parametric study at elevated temperatures, as shown in Figs. 10 and 11 for stub and long columns respectively. It can be observed in the figures that the European standard [14] provides conservative predictions for the strength of both stub and long columns with box and H-sections. The P_{EC} of all box and H-section stub columns was, on average, 17% and 15% lower than the strength estimated in FEA respectively with the corresponding Coefficient of Variation (COV) of 0.16 and 0.16, as shown in Table 5. The strength from parametric study for class 1-3 and class 4 section stub columns is separately compared with the design strength, as shown in Tables 6 and 7 respectively. As can be observed in Table 6, the

design strength predicted for class 1-3 box and H-section compared well with the strength obtained in FEA. The mean values of P_{FEA}/P_{EC} ratios equal to 1.05 and 1.00, with the corresponding COV of 0.04 and 0.01 for class 1-3 box and H-sections, respectively. As for the class 4 section stub columns, the mean values of P_{FEA}/P_{EC} ratios equal to 1.23 and 1.23, with the corresponding COV of 0.16 and 0.13 for box and H-sections, respectively. Thus, the conservatism and scattering of the strength prediction of stub columns was due to the underestimation of the strength of class 4 section stub columns. For the box and H-section long columns, the P_{EC} was, on average, 31% and 39% lower than the strength estimated in FEA respectively with the corresponding COV of 0.08 and 0.07, as shown in Table 8.

5.1.2 AISC standard

The AISC standard [15] was also used to estimate the design strength (P_{AISC}) for columns at elevated temperatures. According to the standard, the strength of the structural member at elevated temperatures can be estimated based on the critical stresses using the material properties at elevated temperatures, as given as Eq. (5), in which $P_{n,T}$ is the nominal compressive strength at temperature T ^{o}C, $F_{cr,T}$ is the critical stress at temperature T ^{o}C, A_g is the gross cross-sectional area of member and A_e is the effective area of the cross-section. The $F_{cr,T}$ for members at elevated temperatures can be calculated from Eq. (6) [38], in which the $f_{e,T}$ is the elastic buckling stress at temperature T ^{o}C.

$$P_{n,T} = \begin{cases} F_{cr,T} * A_g, for\ members\ without\ slender\ elements \\ F_{cr,T} * A_e, for\ members\ with\ slender\ elements \end{cases} \quad (5)$$

$$F_{cr,T} = [0.42^{\sqrt{f_{y,T}/f_{e,T}}}]f_{y,T} \quad (6)$$

The comparison of P_{AISC} estimated using Eqs. (5) and (6) for box section and H-section stub columns with the P_{FEA} of the columns is presented in Figs. 10(a) and 10(b) respectively. As can be seen in the figures, the design strength for stub columns was conservatively predicted. The mean value of P_{FEA} over P_{AISC} for box section stub columns is equal to 1.15 with the COV of 0.10 while the mean value of P_{FEA} over P_{AISC} for H-section stub columns is equal to 1.18 with the COV of 0.10. For long columns, the comparison of the P_{AISC} with the P_{FEA} is presented in Figs. 11(a) and 11(b) for box and H-sections respectively. As can be observed in the figures, the strength prediction for the long columns at elevated temperatures is quite conservative. The mean values of the P_{FEA} over P_{AISC} ratios are respectively 1.43 with a COV of 0.18 for box section long columns, and 1.73 with a COV of 0.11 for H-section long columns. Compared with the European standard, the AISC standard provides much more conservative strength predictions for the long columns.

5.1.3 Direct strength method

The direct strength method (DSM) developed for the design of cold-formed carbon steel structural members [17-18] was also used to predict the design strength of the columns at elevated temperatures with the substitution of the material properties at the corresponding elevated temperatures. The method considers the elastic instabilities of the structural members and determines the strength of any member as the minimum of the capacities predicted separately for global, local and distortional buckling. Since no distortional buckling behaviour was observed for box and H-section stub and long columns, the design strength (P_{DSM}) of any column subject to axial compression was estimated as the minimum of the nominal strength of the column for global buckling (flexural, torsional, or torsional-flexural buckling), and the nominal strength of the column for local buckling, as shown in Eqs. (7), (8) and (9).

$$P_{DSM} = \min\left(P_{ne,T}, P_{nl,T}\right) \tag{7}$$

$$P_{ne,T} = \begin{cases} \left(0.658^{\lambda_{c,T}^2}\right) A_g f_{y,T} & for\ \lambda_{c,T} \leq 1.5 \\ \left(\frac{0.877}{\lambda_{c,T}^2}\right) A_g f_{y,T} & for\ \lambda_{c,T} > 1.5 \end{cases} \tag{8}$$

$$P_{nl,T} = \begin{cases} P_{ne,T} & for \lambda_{l,T} \leq 0.776 \\ \left[1 - 0.15 * \left(P_{crl,T}/P_{ne,T}\right)^{0.4}\right]\left(P_{crl,T}/P_{ne,T}\right)^{0.4} * P_{ne,T} & for \lambda_{l,T} > 0.776 \end{cases} \tag{9}$$

where $P_{ne,T}$ is the nominal strength for global buckling at temperature T, $P_{nl,T}$ is the nominal strength for local buckling at temperature T, $\lambda_{c,T}$ is the non-dimensional slenderness for $P_{ne,T}$, $P_{crl,T}$ is the elastic critical local buckling load at temperature T, and $\lambda_{l,T}$ is the non-dimensional slenderness for $P_{nl,T}$. Tables 5 and 8 and Figs. 10 and 11 present the comparison of the estimated P_{DSM} with P_{FEA} for stub and long columns respectively. For box section stub columns, the prediction of the column strength at elevated temperatures was slightly unconservative with the mean P_{DSM}/P_{FEA} ratio of 1.00 and COV of 0.11. The prediction of strength for the H-section stub columns at elevated temperatures was unconservative with the mean P_{DSM}/P_{FEA} ratio of 0.90 and COV of 0.24. This can also be revealed in Fig. 10 that there are data points lying higher than the linear curve which represents the condition that the design strength equals to the strength estimated in FEA for a column. The strength prediction for non-slender and slender section stub columns were also separately evaluated, as summarised in Tables 6 and 7. It is shown that the unconvervative strength prediction was mainly obtained for stub columns with slender cross-sections. As for the long columns, the design predictions by DSM were slightly conservative. The mean values of P_{FEA}/P_{DSM} are 1.09 and 1.18 with the COV of 0.06 and 0.05 for box and H-section long columns respectively. Comparing with the predictions based on European and

AISC standards, the DSM provides more accurate and less scattered strength predictions for long columns at elevated temperatures.

5.2 Modified design rules

The accuracy of using the existing design rules to predict the strength of welded S460 steel columns under compression at elevated temperatures was evaluated and discussed in the previous section. The comparisons presented in Section 5.1 reveal the significant conservatism of the strength prediction provided by European and AISC standards for both stub and long columns and the unconservative prediction of DSM for stub columns. Therefore, modifications are suggested to the current European standard, AISC standard and the direct strength method in order to achieve accurate and safe strength predictions for welded S460 steel columns under compression at elevated temperatures.

5.2.1 Modification to European standard

The high scattering of the P_{EC} for stub columns at elevated temperatures is mainly due to the significant conservatism of the strength prediction for stub columns with class 4 section based on the 0.2% proof stress ($f_{0.2,T}$). This specification was proposed by Ranby [39] by comparing the design predictions using 0.1% and 0.2% proof stress with the strength obtained for class 4 section stub columns made up of normal strength steel under elevated temperature conditions. In order to obtain more accurate design for S460 stub columns, the stresses at 0.5% and 1% strain ($f_{0.5,T}$ and $f_{1.0,T}$ respectively) at temperature T were also used to estimate the strength for the S460 stub columns with class 4 box and H-sections. The mean values of P_{FEA}/P_{EC}, $P_{FEA}/P_{EC,0.5}$ and $P_{FEA}/P_{EC,1.0}$ based on $f_{0.2,T}$, $f_{0.5,T}$ and $f_{1.0,T}$ respectively are 1.23, 1.14 and 1.08 with the COV of 0.16, 0.09 and 0.07 for class 4 box section stub columns. As for the class 4 H-section stub columns, the mean values of P_{FEA}/P_{EC}, $P_{FEA}/P_{EC,0.5}$ and $P_{FEA}/P_{EC,1.0}$ based on $f_{0.2,T}$, $f_{0.5,T}$ and $f_{1.0,T}$ respectively are 1.23, 1.16 and 1.12 with the COV of 0.13, 0.10 and 0.07. The comparison between the predictions using $f_{0.2,T}$, $f_{0.5,T}$ and $f_{1.0,T}$ reveal that $f_{1.0,T}$ stress can be used to obtain more economical design of the structures. By using the $f_{1.0,T}$ for estimating P_{EC} for class 4 sections, the mean values of $P_{FEA}/P_{EC,mod}$ calculated for stub columns including both Class 1-3 and Class 4 sections are 1.07 and 1.08 with COV of 0.06 and 0.08 for box and H-section structures respectively. The mean values of $P_{FEA}/P_{EC,mod}$ for Class 1-3 section stub columns were about the same as those of P_{FEA}/P_{EC} since the modification was applied to Class 4 section stub columns.

In order to obtain the appropriate buckling curve for columns subject to elevated temperatures, the variation of normalised P_{FEM} by $A_g*f_{y,T}$ with the $\bar{\lambda}_T$ for the box and H-section columns at elevated temperatures was investigated. The $P_{FEA}/ A_g*f_{y,T}$ versus $\bar{\lambda}_T$ is plotted in Fig. 12. As can be seen in the figure, the data points of $P_{FEA}/ A_g*f_{y,T}$ are well above the buckling curve based on the value of β as

0.65 which was obtained by curve-fitting the experimental results of the non-dimensional buckling coefficient with $\bar{\lambda}_T$ for columns with steel grade below 350MPa [37]. In order to achieve safe and more economical design, a buckling curve developed with the value of β as 0.3 was proposed for the strength prediction of welded S460 box and H-section columns at elevated temperatures. The comparison of the $P_{FEA}/ A_g*f_{y,T}$ results with the proposed design curve is also shown in Fig. 12. As shown in the figure, the proposed buckling curve compared better with the $P_{FEA}/ A_g*f_{y,T}$ results than the original buckling curve. Based on the proposed buckling curve, the mean values of $P_{FEA}/P_{EC,mod}$ are 1.12 and 1.17, with the COV of 0.06 and 0.05, for box and H-section long columns, respectively. Comparing with the strength predictions using the buckling curve from European standard based on the value of 0.65 for β, the proposed design curve provides more accurate and less scattering strength predictions, as shown in Table 8.

5.2.2 Modification to the AISC standard

The AISC design strength predictions for columns were primarily based on the critical stress (F_{cr}) estimated using Eq. (6). This equation developed by curve-fitting the compressive strength of normal strength steel columns at elevated temperatures [38] may be unsuitable for estimating the critical stress of high strength steel structures. In the modification of AISC standard, the variation of the normalised column strength ($P_{n,FEA}$) obtained using FEA results, with the $f_{y,T}/f_{e,T}$ was plotted and used. Eq. (10) for estimating F_{cr} at elevated temperatures was obtained as the lower bound of the normalised column strength for any value of $f_{y,T}/f_{e,T}$, as shown in Fig. 13.

$$F_{cr} = \left[0.65^{(f_{y,T}/f_{e,T})}\right] f_{y,T} \tag{10}$$

The improvement of the accuracy for the design strength predictions can be revealed by comparing the mean values and scattering of the $P_{FEA}/P_{AISC,mod}$ with those of the P_{FEA}/P_{AISC} for stub and long columns with box and H-sections, as shown in Tables 5-8.

5.2.3 Modification to the direct strength method

Modification to DSM for accurately estimating the strength of stub columns considering local buckling at elevated temperatures was conducted based on the strength obtained in the parametric study for the stub columns with different $\lambda_{l,T}$. The normalised P_{FEM} by $P_{ne,T}$ for the box and H-section stub columns at elevated temperatures is plotted versus the $\lambda_{l,T}$, as shown in Fig. 14. As can be seen in the figure, the variation of $P_{FEM}/P_{ne,T}$ with $\lambda_{l,T}$ follows a clear trend. The Eq. (11) obtained through regression analysis is proposed for estimating the nominal strength of the column for local buckling

($P_{nl,T}$) at elevated temperatures. The equation can be used together with Eqs. (7) and (8) to determine the compressive strength of any welded S460 box and H-section column at elevated temperatures.

$$P_{nl,T} = \begin{cases} P_{ne,T} & for \lambda_{l,T} \leq 0.707 \\ \left[0.96 * \left(\frac{P_{crl,T}}{P_{ne,T}}\right)^{0.45} - 0.22 * \left(\frac{P_{crl,T}}{P_{ne,T}}\right)^{0.5}\right] * P_{ne,T} & for \lambda_{l,T} > 0.707 \end{cases} \quad (11)$$

Comparisons of the strength predicted using this modified DSM approach ($P_{DSM,mod}$) with both P_{FEA} from parametric study and P_{DSM} based on the original DSM for stub columns at elevated temperatures are presented in Fig. 14 and Tables 5-7. As revealed in the Fig. 14, the modified DSM approach is more accurate and conservative to predict the compressive strength for the Class 4 section stub columns with relatively high $\lambda_{l,T}$ values. For box and H-section stub columns respectively, the mean values of P_{FEA}/ $P_{DSM,mod}$ equal to 1.08 and 1.07, with COV of 0.08 and 0.08 are compared with the mean values of P_{FEA}/ P_{DSM} equal to 1.00 and 0.90, with COV of 0.11 and 0.24. Therefore, the modified DSM provides conservative predictions with a lower scattering than the predictions of original DSM for stub columns under elevated temperature conditions. As for the long columns with box and H-sections respectively, the $P_{DSM,mod}$ for the columns are the same as the P_{DSM} estimated based on the original DSM because no strength reduction due to local buckling was obtained for these columns with non-slender cross-sections.

6. Conclusions

Axial compressive strength of welded S460 steel box and H-section columns at elevated temperatures was investigated using finite element analysis. A stress-strain curve model for S460 steel at various elevated temperatures was proposed to obtain accurate stress-strain relationship of S460 for structural design and analysis. A finite element model was developed with the incorporation of the stress-strain curves obtained based on the proposed model and validated using the experimental results of the ultimate compressive strength, load-deformation behaviour and failure modes of welded S460 steel columns with box and H-sections at room and elevated temperatures. A parametric study was carried out to determine the compressive strength of fixed-ended stub columns and pin-ended long columns with varying cross-sectional slenderness and column slenderness ratios at elevated temperatures.

The results of parametric study were compared with the design strength calculated according to the current European and AISC standards for structures subject to elevated temperatures as well as the original direct strength method, with the substitution of material properties at elevated temperatures. The European standard generally provides conservative predictions for the design strength of both stub and long columns with box and H-sections while the AISC standard significantly underestimates the strength of the columns. The original direct strength method overestimates the strength of stub

columns at elevated temperatures while provides the most accurate predictions for long columns comparing with the predictions from both European and AISC standards. Modifications to the current design rules in European and AISC standards and original direct strength method have been proposed. The modified design rules are found to provide more accurate predictions for welded S460 steel box and H-section columns at elevated temperatures. Therefore, the modified design rules are recommended to be used for predicting the strength of welded S460 box and H-section columns at elevated temperatures for structural design.

Acknowledgements

The authors are grateful for the support from the Chinese National Engineering Research Centre for Steel Construction (Hong Kong Branch) at the Hong Kong Polytechnic University.

References

[1] Shi, G., Zhou, W.J., Bai, Y. and Lin, C.C. 2014. Local buckling of 460 MPa high strength steel welded section stub columns under axial compression. *Journal of Constructional Steel Research*, 100, 60-70.

[2] Shi, G., Zhou, W.J. and Lin, C.C. 2015. Experimental investigation on local buckling behaviour of 960 MPa high strength steel welded section stub columns. *Advances in Structural Engineering*, 18, 423-437.

[3] Ma, J.L., Chan, T.M. and Young, B. 2016. Experimental investigation on stub-column behaviour of cold-formed high strength steel tubular sections. *Journal of Structural Engineering*, 142, 04015174.

[4] Yang, D.M. and Hancock, G.J. 2006. Numerical simulation of high-strength steel box-shaped columns failing in local and overall buckling modes. *Engineering Structures*, 132, 541-549.

[5] Rasmussen, K.J.R. and Hancock, G.J. 1995. Test of high strength steel columns. *Journal of Constructional Steel Research*, 34, 27-52.

[6] Yoo, J.H., Kim, J.W., Yang, J.G., Kang, J.W. and Lee, M.J. 2013. Local buckling in the stub columns fabricated with HSA800 of high performance steel. International *Journal of Steel Structures*, 34, 445-458.

[7] Chan, T.M., Zhao, X.L. and Young, B. 2015. Cross-section classification for cold-formed and built-up high strength carbon and stainless steel tubes under compression. *Journal of Constructional Steel Research*, 106, 289-295.

[8] Wang, Y.B., Li, G.Q., Chen, S.W. and Sun, F.F. 2012. Experimental and numerical study on the behavior of axially compressed high strength steel columns with H-section. *Engineering Structures*, 43, 149-159.

[9] Wang, Y.B., Li, G.Q., Chen, S.W. and Sun, F.F. 2014. Experimental and numerical study on the behavior of axially compressed high strength steel box-columns. *Engineering Structures*, 58, 79-91.

[10] Ban, H.Y., Shi, G., Shi, Y.J. and Bradford, M.A. 2013. Experimental investigation of the overall buckling behaviour of 960 MPa high strength steel columns. *Journal of Constructional Steel Research*, 88, 256-266.

[11] Li, T.J., Li, G.Q., Chan, S.L. and Wang, Y.B. 2016. Behavior of Q690 high-strength steel columns: Part1: Experimental investigation. *Journal of Constructional Steel Research*, 123, 18-30.

[12] Li, T.J., Liu, S.W., Li, G.Q., Chan, S.L. and Wang, Y.B. 2016. Behavior of Q690 high-strength steel columns: Part2: Parametric study and design recommendation. *Journal of Constructional Steel Research*, 122, 379-394.

[13] Chen, J. and Young, B. 2008. Design of high strength steel columns at elevated temperatures. *Journal of Constructional Steel Research*, 64, 689-703.

[14] EN 1993-1-2, 2005. *Eurocode 3: Design of steel structures-Part 1-2: General rules-structural fire design*. Brussels: European Committee for Standardization.

[15] ANSI/AISC 360-16, 2016. *Specification for structural steel buildings*. AISC, Chicago.

[16] Ma, J.L., Chan, T.M. and Young, B. 2015. Material properties and residual stresses of cold-formed high strength steel hollow sections. *Journal of Constructional Steel Research*, 109, 152-165.

[17] Schafer, B.W. 2002. Local, distortional, and Euler buckling of thin-walled columns. *Journal of Structural Engineering*, ASCE, 128, 289-299.

[18] Li, Z. and Schafer, B.W. 2010. Application of the finite strip method in cold-formed steel member design. *Journal of Constructional Steel Research*, 66, 971-980.

[19] Wang, W.Y., Kodur, V., Yang, X.C. and Li, G.Q. 2014. Experimental study on the local buckling of axially compressed steel stub columns at elevated temperatures. *Thin-Walled Structures*, 82, 33-45.

526 [20] Qiang, X.H., Bijlaard, F.S.K. and Kolstein, H. 2013. Elevated-temperature mechanical properties
527 of high strength structural steel S460N: Experimental study and recommendations for fire-resistance
528 design. *Fire Safety Journal*, 55, 15-21.

529 [21] Ban, H.Y., Shi, G., Shi, Y.J. and Wang, Y.Q. 2012. Overall buckling behaviour of 460 MPa high
530 strength steel columns: Experimental investigation and design method. *Journal of Constructional*
531 *Steel Research*, 74, 140-150.

532 [22] Schneider, R. and Lange, J. 2011. Constitutive equations and empirical creep law of structural
533 steel S460 at high temperatures. *Journal of Structural Fire Engineering*, 2, 217-229.

534 [23] Ramberg, W. and Osgood, W.R. 1943. Description of stress-strain curves by three parameters.
535 *NACA Technical Note 902*.

536 [24] Olawale, A.O. and Plank, R.J. 1988. The collapse analysis of steel columns in fire using a finite
537 strip method. *International Journal for Numerical Methods in Engineering*, 26, 2755-2764.

538 [25] Outinen, J., Kesti, J. and Mäkeläinen, P. 1996. Behaviour of high-strength structural steel S420M
539 at elevated temperatures. *Rakenteiden Mekaniikka*, 29, 103-114.

540 [26] Lee, J.H., Mahendran, M. and Makelainen, P. 2003. Prediction of mechanical properties of light
541 gauge steels at elevated temperatures. *Journal of Constructional Steel Research*, 59, 1517-1532.

542 [27] Mirambell, E. and Real, E. 2000. On the calculation of deflections in structural stainless steel
543 beams: an experimental and numerical investigation. *Journal of Constructional Steel Research*, 54,
544 109-133.

545 [28] ABAQUS [Computer software] (2013). Dassault Systèmes, Providence, RI.

546 [29] Wang, Y.B., Li, G.Q. and Chen, S.W. 2012. The assessment of residual stresses in welded high
547 strength steel box sections. *Journal of Constructional Steel Research*, 76, 93-99.

548 [30] Wang, Y.B., Li, G.Q. and Chen, S.W. 2012. Residual stresses in welded flame-cut high strength
549 steel H-sections. *Journal of Constructional Steel Research*, 79, 159-165.

550 [31] EN 1993-1-1, 2005. *Eurocode 3: Design of steel structures - Part 1-1: General rules and rules*
551 *for buildings*. Brussels: European Committee for Standardization.

552 [32] Dong, P.S., Song, S.P. and Zhang, J.M. 2014. Analysis of residual stress relief mechanisms in
553 post-weld heat treatment. *International Journal of Pressure Vessels and Piping*, 122, 6-14.

554 [33] Yang, K.C., Lee, H.H. and Chan, O. 2006. Experimental study of fire-resistant steel H-columns
555 at elevated temperatures. *Journal of Constructional Steel Research*, 62, 544-553.

556 [34] Ng, K.T. and Gardner, L. 2007. Buckling of stainless steel columns and beams in fire.
557 *Engineering Structures*, 29, 717-730.

558 [35] Franssen, J.M., Kodur, V. and Zaharia, R. 2009. *Designing steel structures for fire safety*. CRC
559 Press.

560 [36] Heidarpour, A., Cevro, S., Song, Q.Y. and Zhao, X.L. 2014. Behaviour of stub columns utilising
561 mild-steel plates and VHS tubes under fire. *Journal of Constructional Steel Research*, 95, 220-229.

562 [37] Franssen, J.M., Talamona, D., Kruppa, J. and Cajot, L.G. 1998. Stability of steel columns in case
563 of fire: experimental evaluation. *Journal of Constructional Steel Research*, 124, 158-163.

564 [38] Takagi, J. and Deierlein, G.G. 2007. Strength design criteria for steel members at elevated
565 temperatures. *Journal of Constructional Steel Research*, 63, 1036-1050.

566 [39] Ranby, A. 1998. Structural fire design of thin walled steel sections. *Journal of Constructional*
567 *Steel Research*, 46, 303-304.

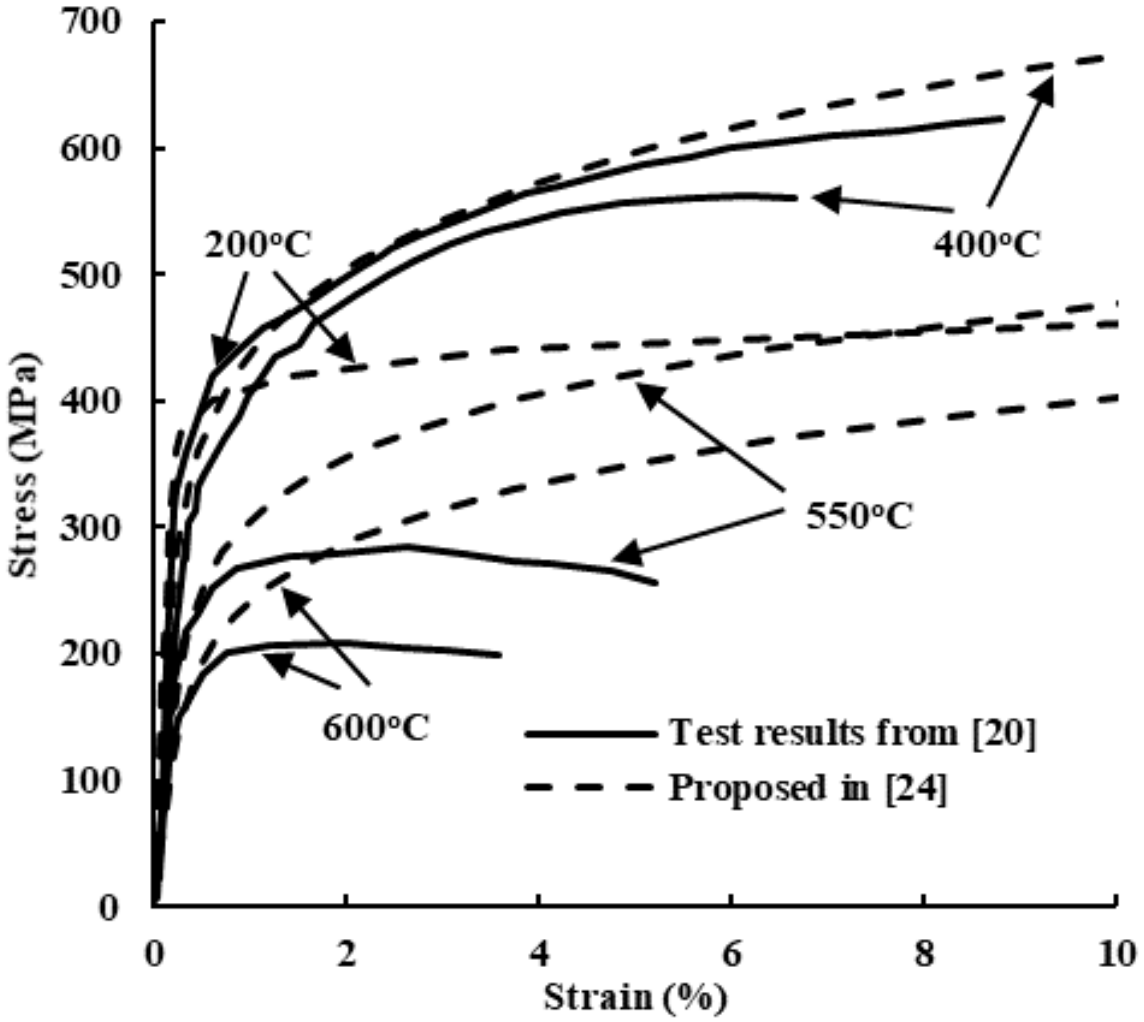

Figure 1. Comparison of stress-strain curves predicted using the model in [24] with the test results from [20].

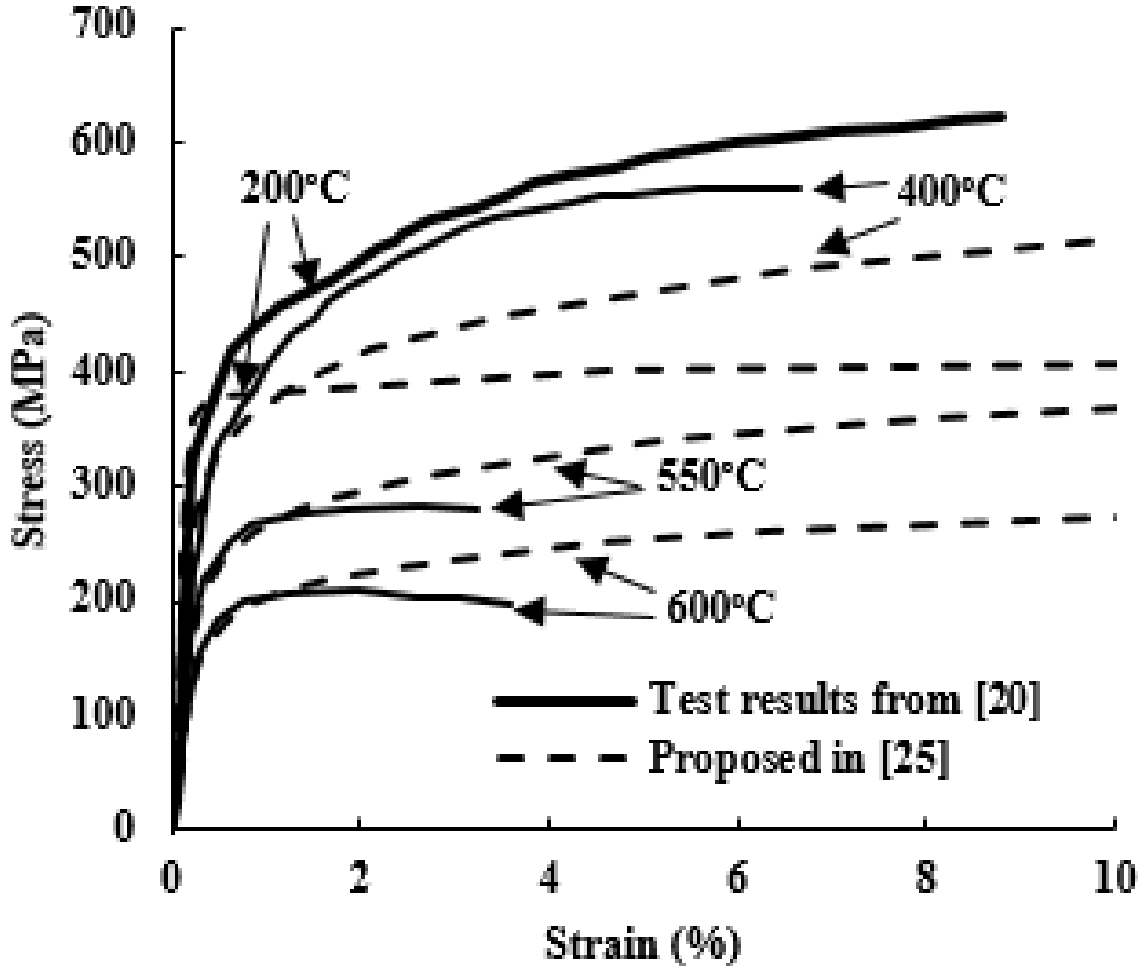

Figure 2. Comparison of stress-strain curves predicted using the model in [25] with the test results from [20].

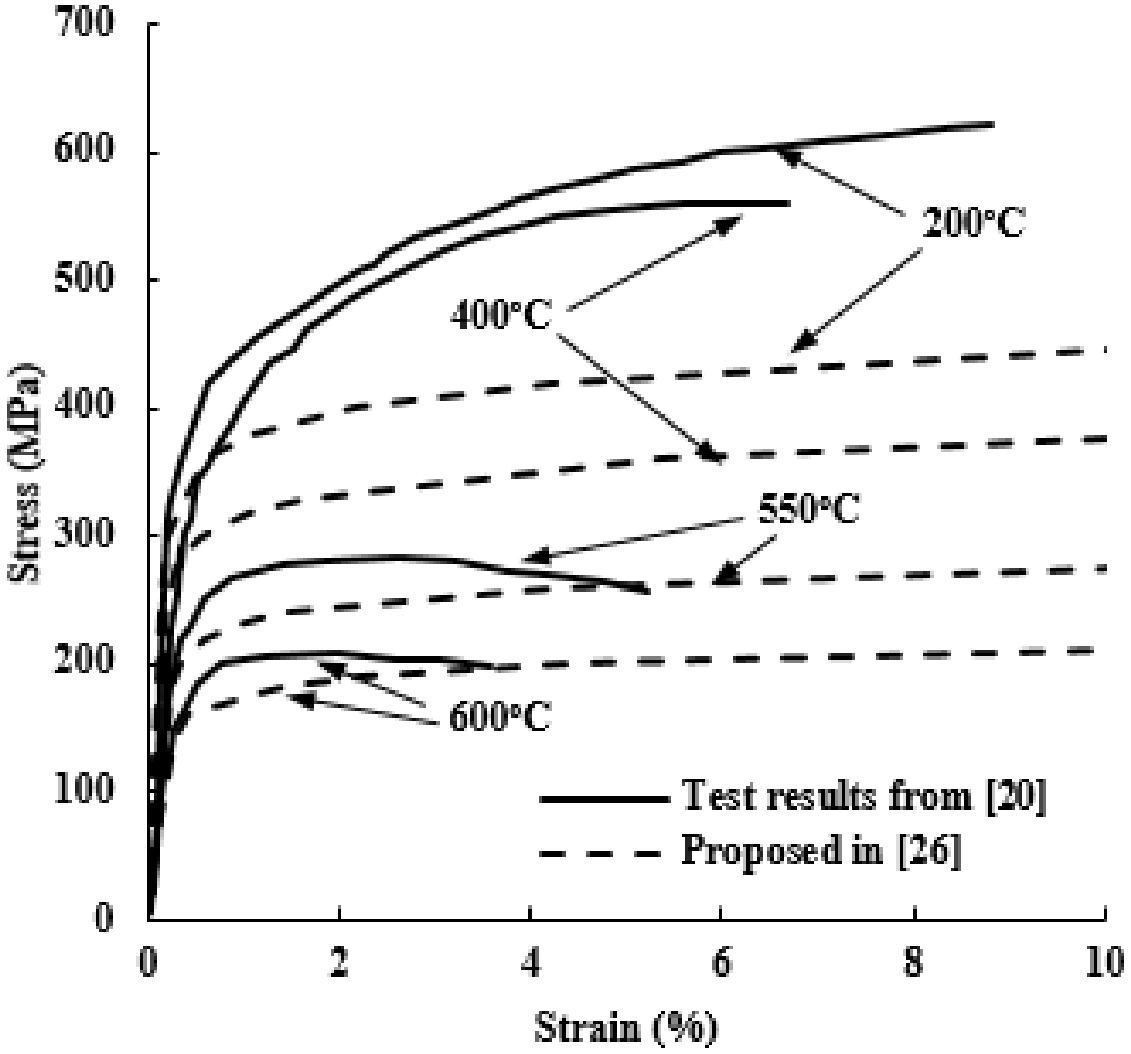

Figure 3. Comparison of stress-strain curves predicted using the model proposed by Lee and the co-workers [26] with the test results [20].

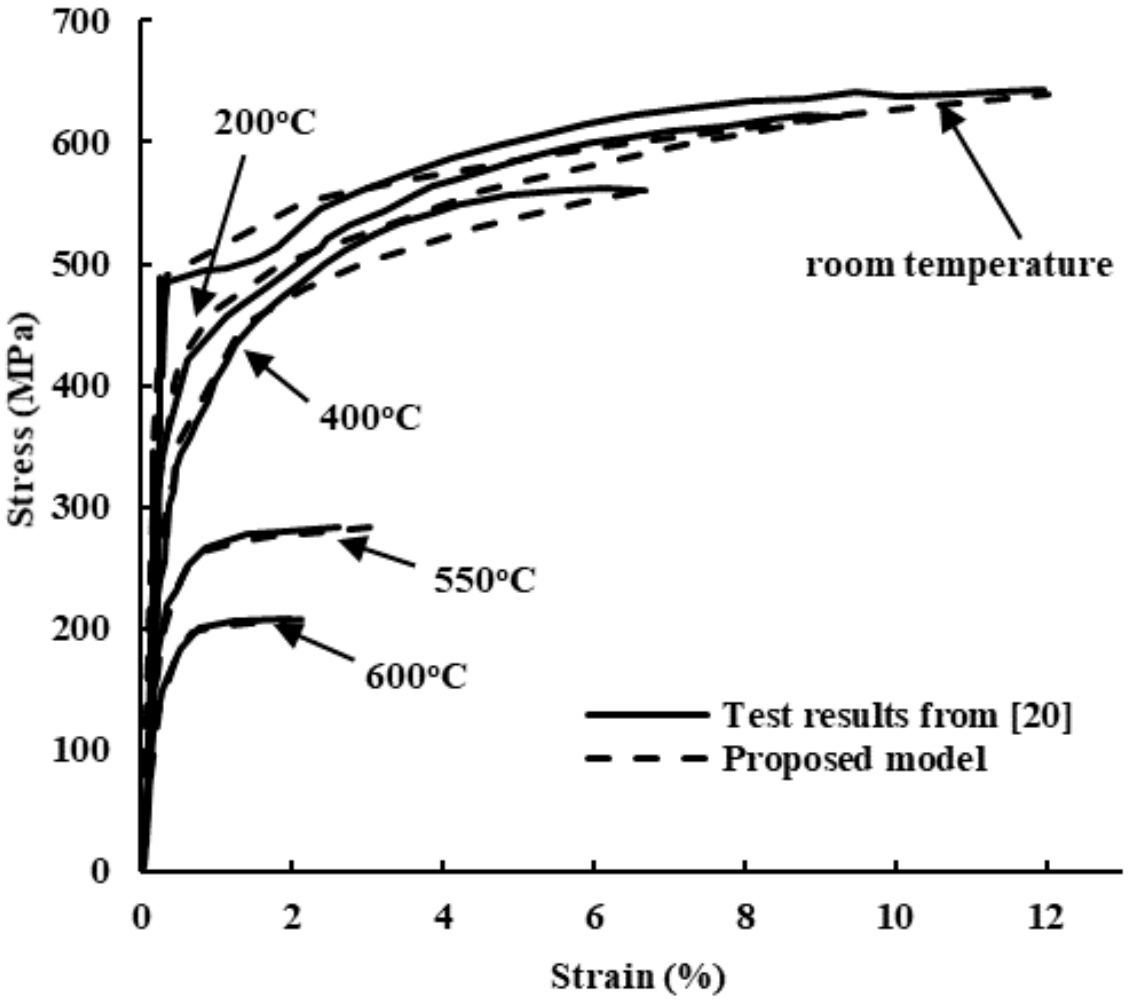

Figure 4. Comparing the new stress-strain model to experimental results from [20]

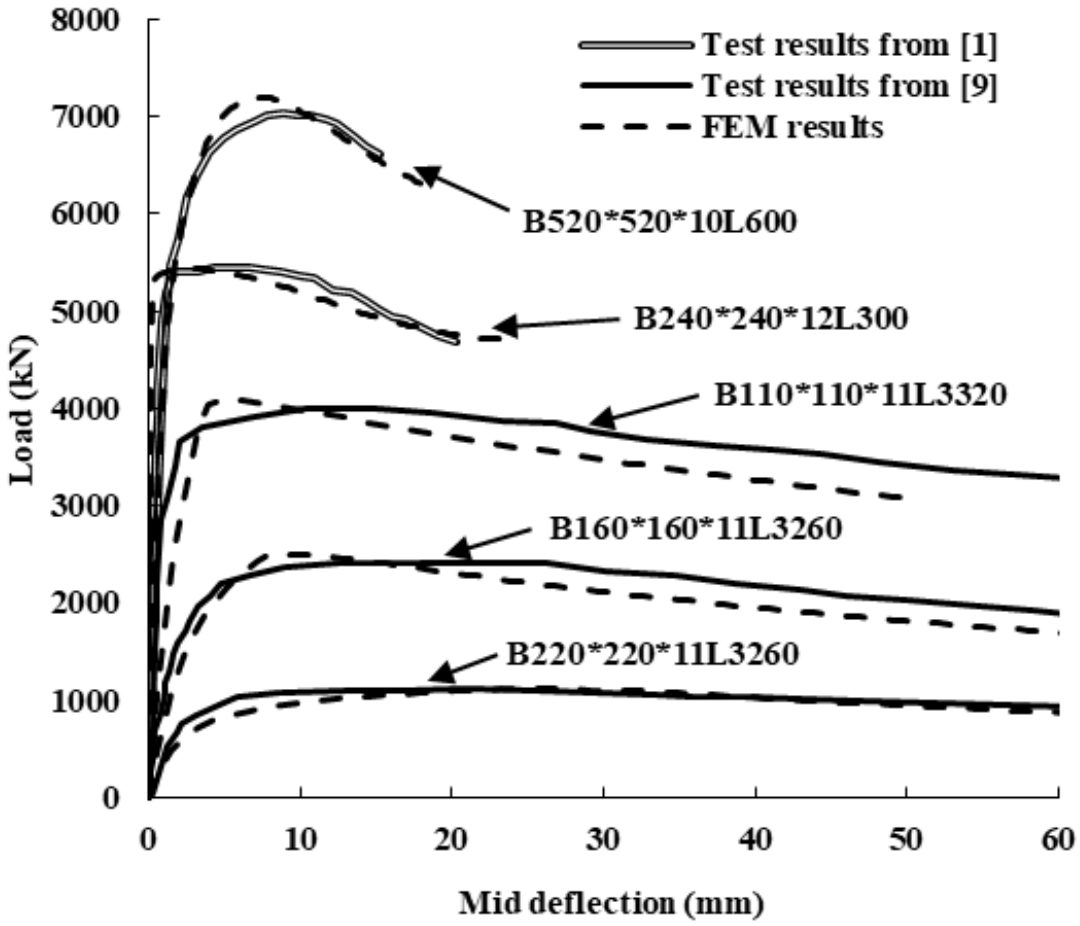

Figure 5. Comparison of the load-deflection curves obtained from experiments conducted at room temperature with those from FEM for box-section columns.

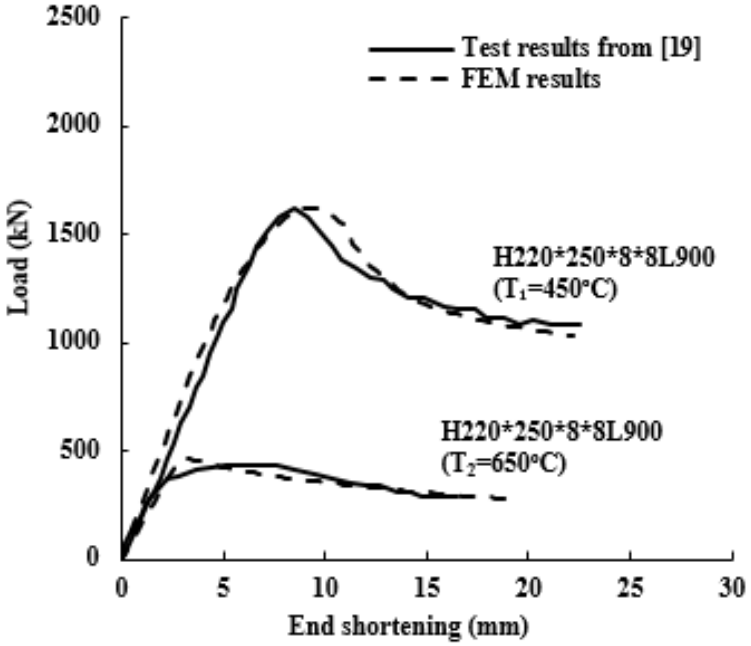

(a)

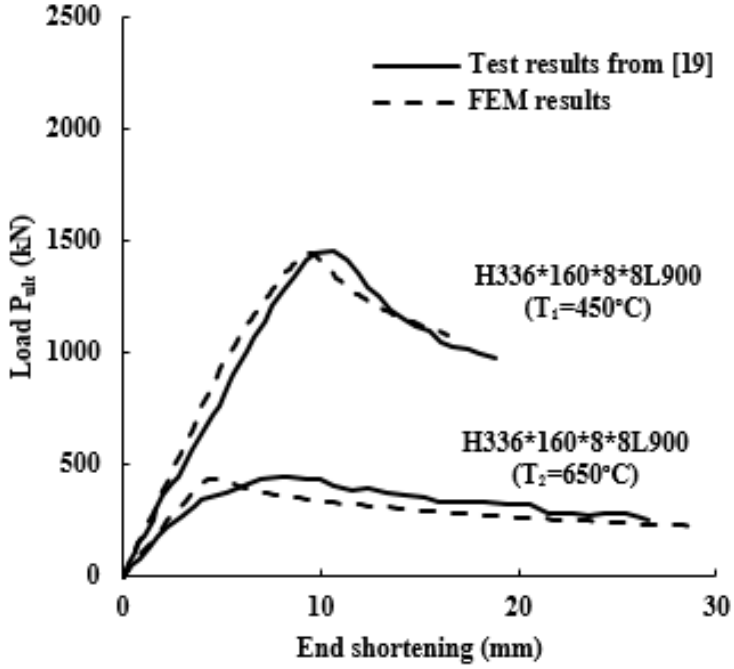

(b)

Figure 6. Comparison of the load-end shortening curves obtained from experiments with those from FEM for (a) H220*250*8*8L900 columns and (b) H336*160*8*8L900 columns.

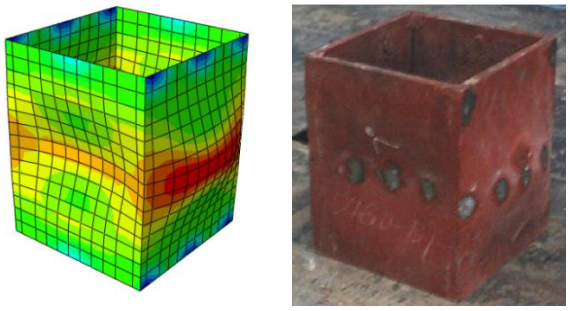

(a)

(b)

(c)

Figure 7/14

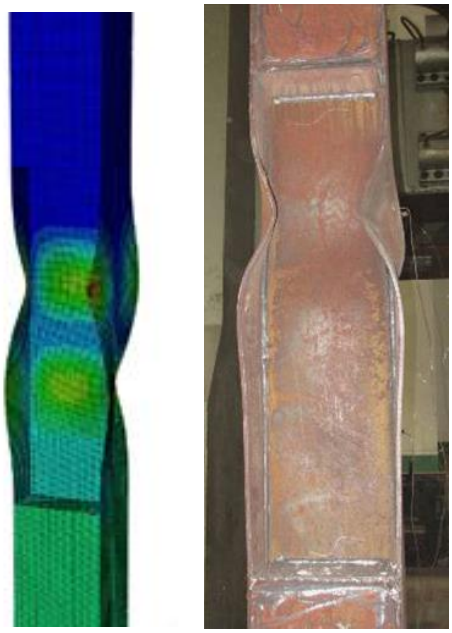

(d)

Figure 7. Comparison of the deformation and failure mode obtained in experiments and finite element analysis for (a) B240*240*12L300 with local buckling failure [1]; (b) B110*110*11L3320 with flexural buckling failure [9]; (c) H160*170*21*11L3304 with flexural buckling about minor axis [8]; (d) H220*250*8*8L900 (T_1=450^{o}C) with local buckling failure [19].

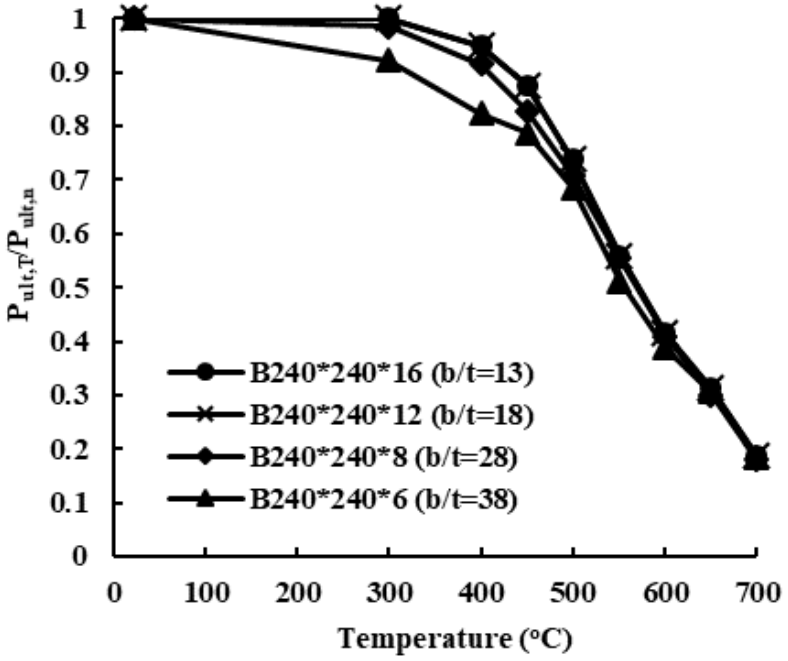

(a)

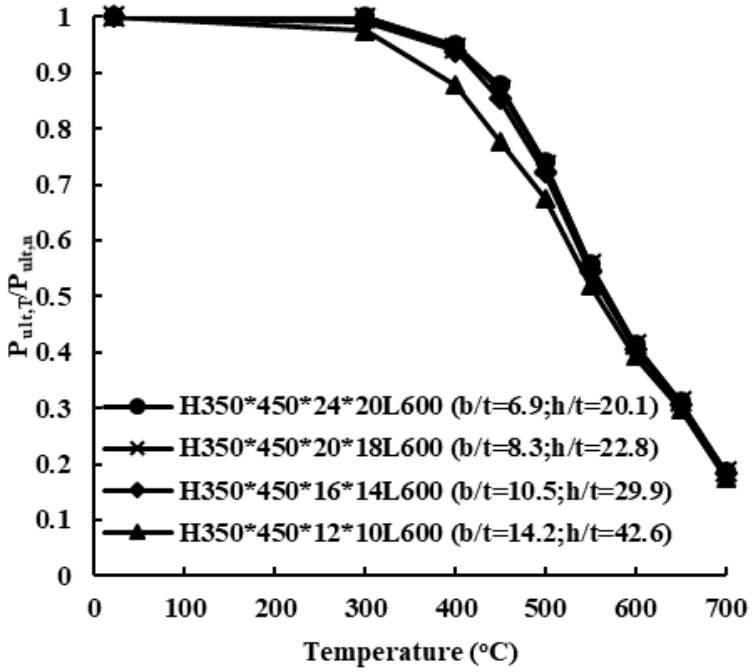

(b)

Figure 8. Effects of cross sectional slenderness and temperature on the $P_{ult,T}/ P_{ult,n}$ for (a) box section stub columns and (b) H-section stub columns.

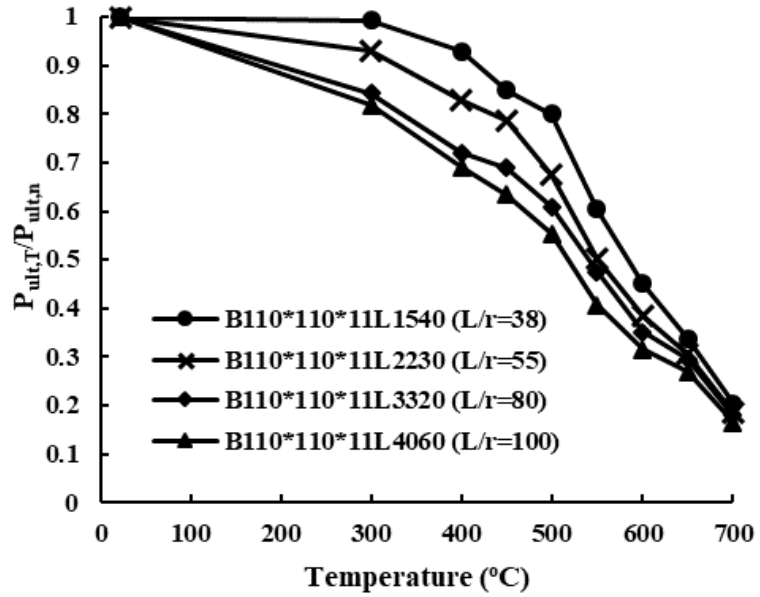

(a)

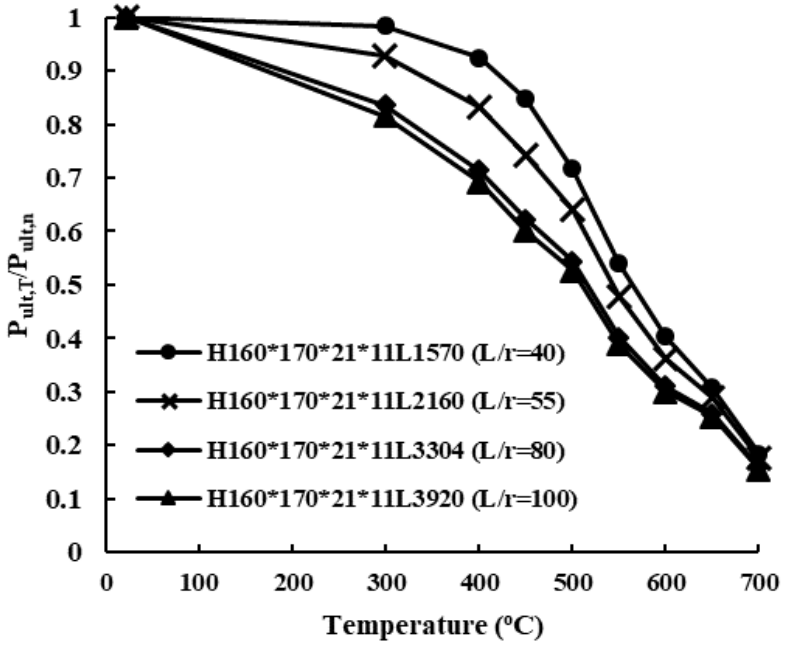

(b)

Figure 9. Effects of column slenderness ratio and temperature on the $P_{ult,T}/ P_{ult,n}$ for (a) box section and (b) H-section long columns.

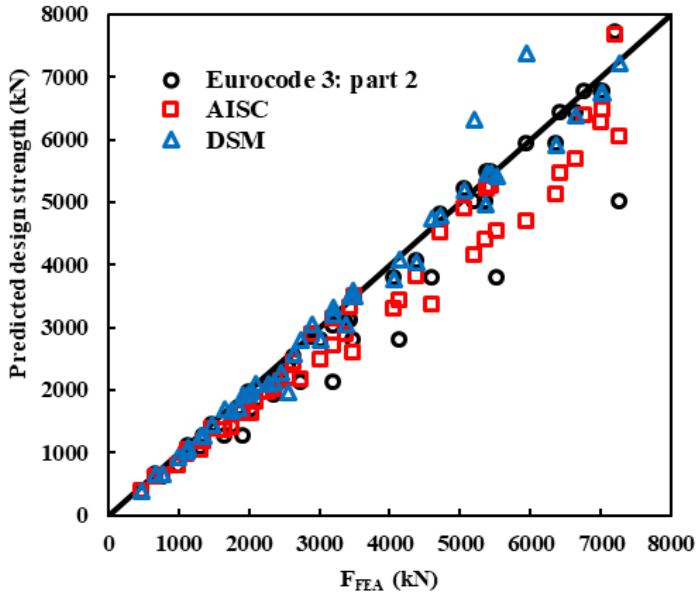

(a)

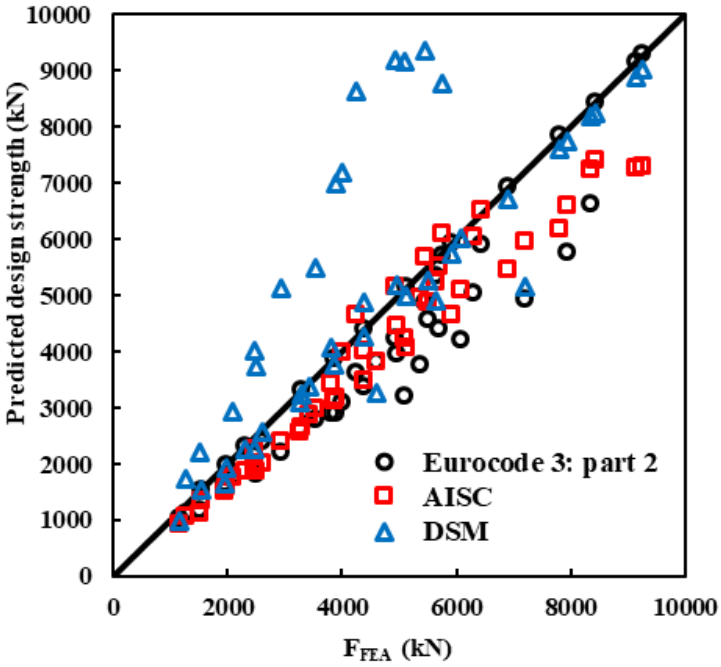

(b)

Figure 10. Comparison of the strength estimated using FEA and design strength based on European standard [14], American standard [15] and DSM for stub columns with (a) box section and (b) H-section.

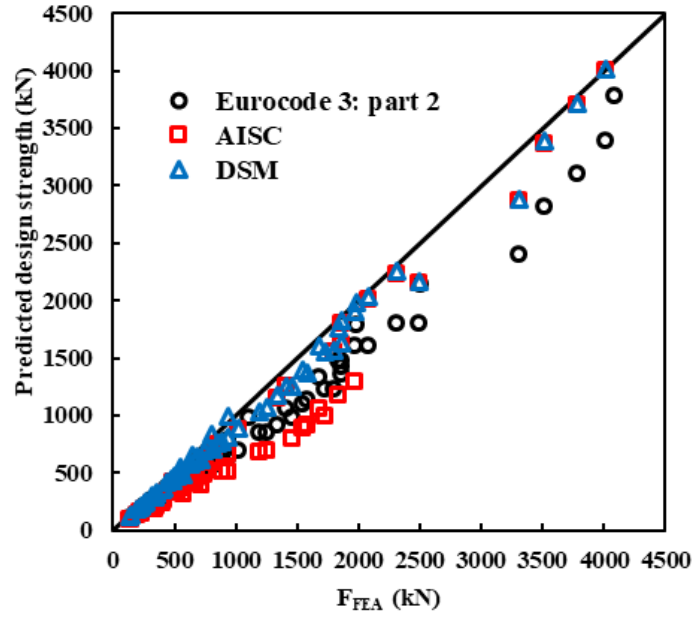

(a)

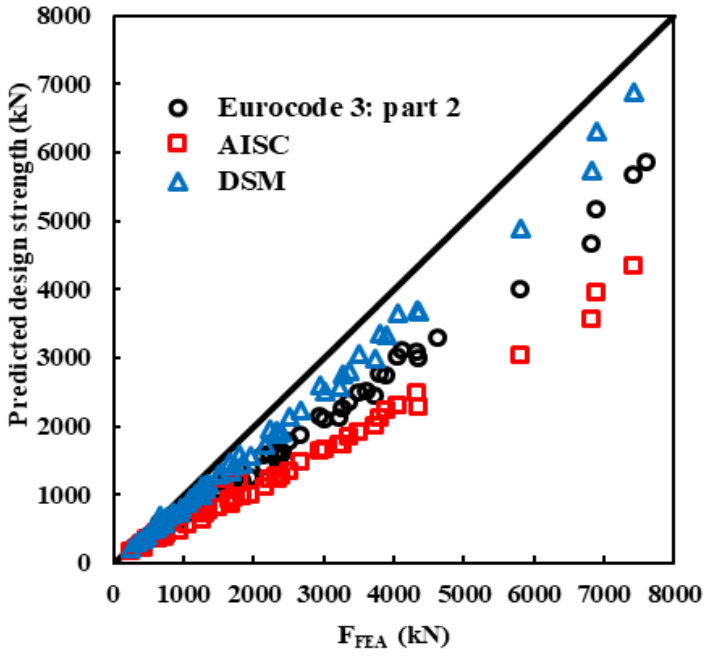

(b)

Figure 11. Comparison of the strength estimated using FEA and design strength based on European standard [14], American standard [15] and DSM for long columns with (a) box section and (b) H-section.

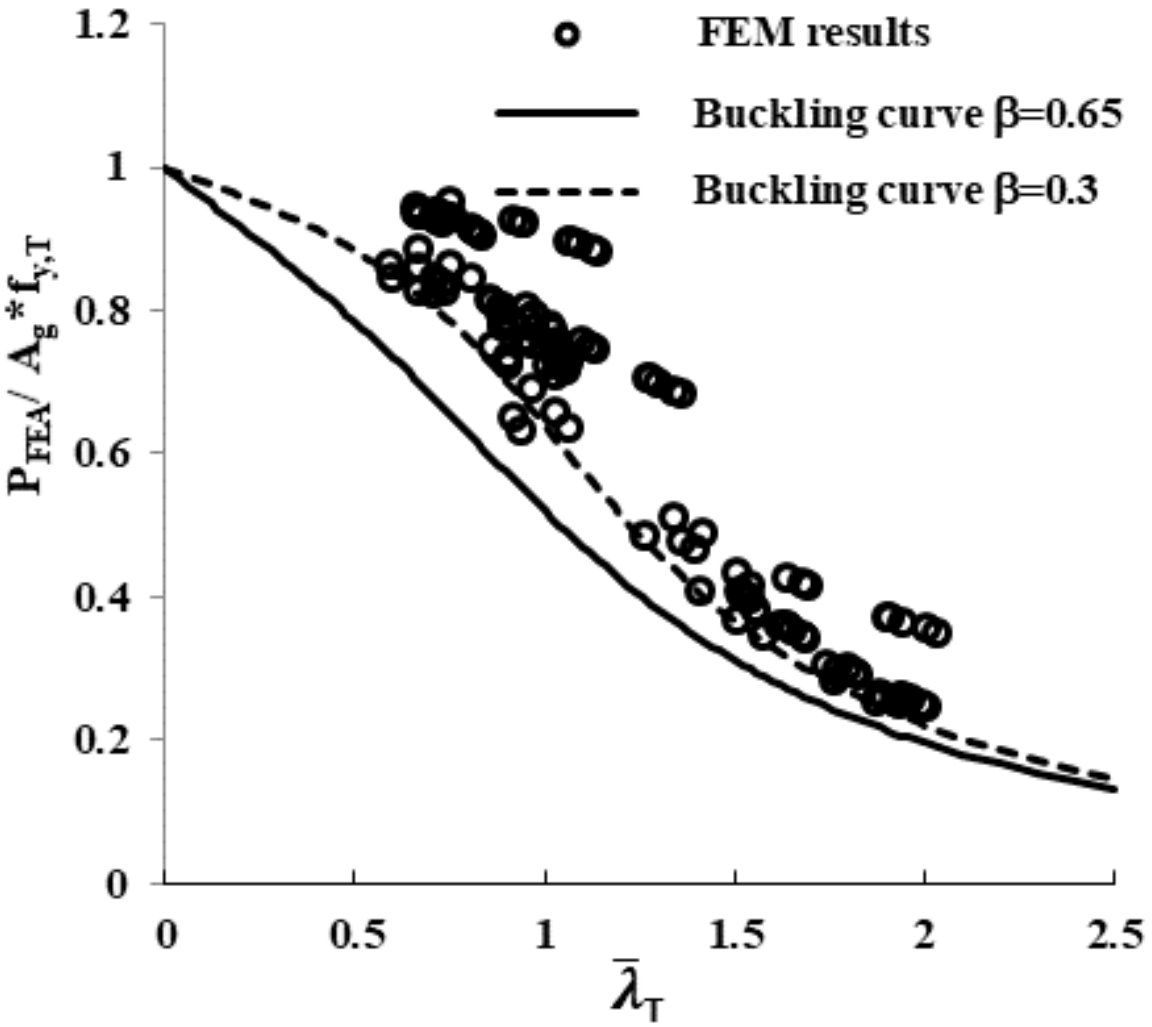

Figure 12. Buckling curves and the variation of $P_{FEA}/ A_g*f_{y,T}$ with $\bar{\lambda}_T$.

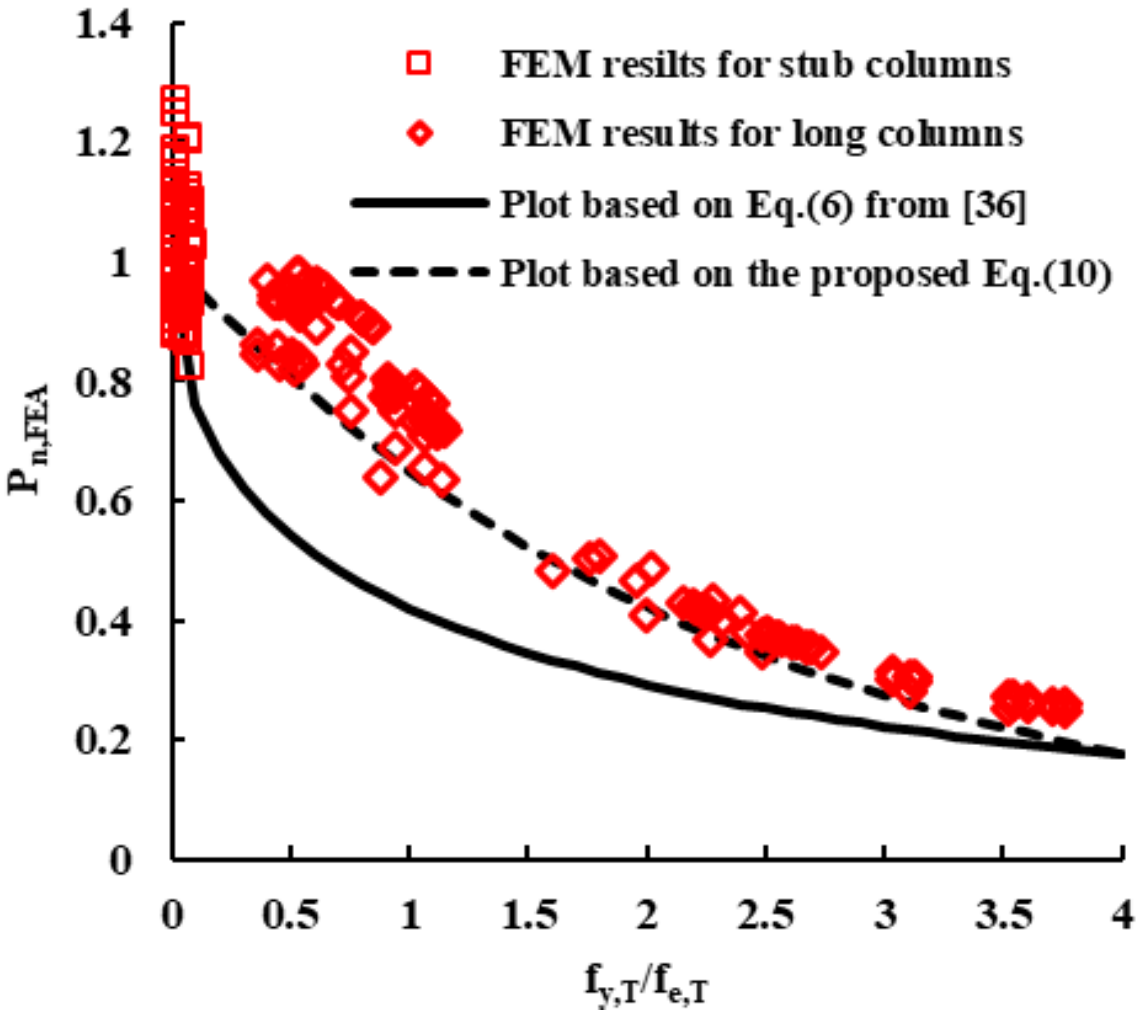

Figure 13. Variation of normalised column strength from FEA ($P_{n,FEA}$) with $f_{y,T}/f_{e,T}$.

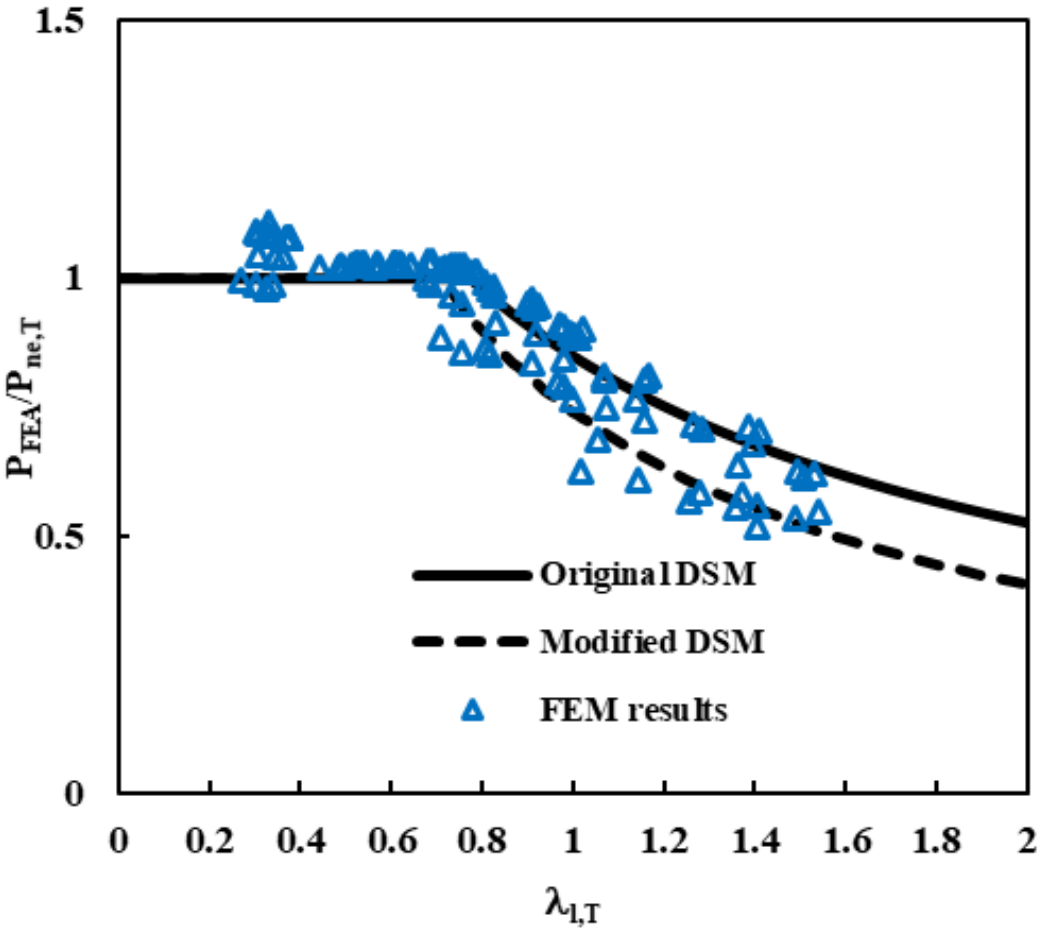

Figure 14. Comparison of the strength estimated using FEA and design strength based on modified DSM approach and current DSM for stub columns with box and H-section.

Table 1. Comparison between tests and finite element analysis (FEA) results.

Specimen	Boundary conditions	Test results		FEA results		Comparison
		$P_{ult,test}$ (kN)	Failure mode	$P_{ult,FEA}$ (kN)	Failure mode	$P_{ult,FEA}/P_{ult,test}$
B240*240*12L300[1]	Fixed	5460	L	5436	L	0.99
B430*430*12L500[1]	Fixed	8923	L	8902	L	1.00
B520*520*10L600[1]	Fixed	7035	L	7200	L	1.02
B100*100*10L4520[21]	Pinned	931	F	909	F	0.98
B110*110*11L3320[9]	Pinned	1123	F	1125	F	1.00
B160*160*11L3260[9]	Pinned	2437	F	2510	F	1.03
B220*220*11L3260[9]	Pinned	4010	F	4090	F	1.02
H350*450*12*10L600[1]	Fixed	5513	L	5647	L	1.02
H490*620*12*10L800[1]	Fixed	5619	L	5743	L	1.02
H590*750*12*10L1000[1]	Fixed	6392	L	6443	L	1.00
H150*150*10*10L2580[21]	Pinned	2438	F	2414	F	0.99
H160*170*21*11L3304[8]	Pinned	2108	F	2149	F	1.02
H230*250*21*11L3320[8]	Pinned	4358	F	4444	F	1.02
H310*320*21*11L3320[8]	Pinned	7597	F	7615	F	1.00
H220*250*8*8L900 (T_1=450°C)[19]	Fixed	1640	L	1620	L	0.98
H220*250*8*8L900 (T_2=650°C)[19]	Fixed	430	L	460	L	1.06
H336*160*8*8L900	Fixed	1450	L	1446	L	1.00

(T_1=450°C)[19]						
H336*160*8*8L900 (T_2=650°C)[19]	Fixed	430	L	448	L	1.04
Mean						1.01
COV						0.02

Table 1/8

Table 2. Nominal cross-sectional dimensions of stub columns with box and H-sections.

Column	Flange thickness t_f (mm)	Web thickness t_w (mm)	Cross-sectional classification based on Eurocode 3
B240*240L300	6	6	Class 4 (slender)
	8	8	Class 4 (slender)
	12	12	Class 1 (non-slender)
	16	16	Class 1 (non-slender)
B430*430L500	12	12	Class 4 (slender)
B520*520L600	10	10	Class 4 (slender)
H350*450L600	12	10	Class 4 (slender)
	16	14	Class 4 (slender)
	20	18	Class 3 (non-slender)
	24	20	Class 2 (non-slender)
H490*620L800	12	10	Class 4 (slender)
H590*750L1000	12	10	Class 4 (slender)

Table 3. Nominal dimensions and slenderness ratios of long columns with box and H-sections.

Column	**Effective length L_{eff} (mm)**	**L/r**	$\bar{\lambda}$
B110*110*11	1540, 2230, 3260, 4060	38, 55, 80, 100	0.597, 0.865, 1.265, 1.575
B100*100*10	2280	60	0.970
B160*160*11	3260	55	0.865
B220*220*11	3260	38	0.600
H160*170*21*11	1570, 2160, 3304, 3920	40, 55, 80, 100	0.648, 0.890, 1.369, 1.616
H150*150*10*10	1300	36	0.580
H230*250*21*11	3320	55	0.856
H310*320*21*11	3320	40	0.672

Table 4. Reduction factors for mechanical properties of 460MPa steel at elevated temperatures

Temperature (ºC)	**Reduction factor**				
	E	**$f_{2.0}$**	**$f_{0.2}$**	**f_u**	**ε_u**
Room temperature	1	1	1	1	1
300	0.799	1	0.811	1	0.786
400	0.669	0.949	0.736	0.880	0.514
450	0.578	0.877	0.626	0.750	0.326
500	0.509	0.739	0.518	0.601	0.284
550	0.374	0.559	0.491	0.443	0.220
600	0.291	0.415	0.376	0.328	0.166
650	0.248	0.313	0.310	0.249	0.140
700	0.153	0.187	0.197	0.157	0.061

Table 5. Comparison of the strength estimated by FEA with the predicted design strength for all stub columns at elevated temperatures.

	Parameters	P_{FEA}/P_{EC}	$P_{FEA}/P_{EC,mod}$	P_{FEA}/P_{AISC}	$P_{FEA}/P_{AISC,mod}$	P_{FEA}/P_{DSM}	$P_{FEA}/P_{DSM,mod}$
Box section	Mean	1.17	1.07	1.15	1.10	1.00	1.08
	COV	0.16	0.06	0.10	0.08	0.11	0.08
H-section	Mean	1.15	1.08	1.18	1.09	0.90	1.07
	COV	0.16	0.08	0.10	0.09	0.24	0.08

Table 6. Comparison of the strength estimated by FEA with the predicted design strength for class 1-3 (non-slender) stub columns at elevated temperatures.

	Parameters	P_{FEA}/P_{EC}	$P_{FEA}/P_{EC,mod}$	P_{FEA}/P_{AISC}	$P_{FEA}/P_{AISC,mod}$	P_{FEA}/P_{DSM}	$P_{FEA}/P_{DSM,mod}$
Box section	Mean	1.05	1.05	1.14	1.08	1.05	1.05
	COV	0.04	0.04	0.07	0.06	0.04	0.04
H-section	Mean	1.00	1.00	1.25	1.11	1.02	1.04
	COV	0.01	0.01	0.02	0.01	0.01	0.01

Table 7. Comparison of the strength estimated by FEA with the predicted design strength for class 4 (slender) stub columns at elevated temperatures.

	Parameters	P_{FEA}/P_{EC}	$P_{FEA}/P_{EC,mod}$	P_{FEA}/P_{AISC}	$P_{FEA}/P_{AISC,mod}$	P_{FEA}/P_{DSM}	$P_{FEA}/P_{DSM,mod}$
Box section	Mean	1.23	1.08	1.16	1.12	0.99	1.11
	COV	0.16	0.07	0.11	0.08	0.13	0.09
H-section	Mean	1.23	1.12	1.14	1.09	0.83	1.09
	COV	0.13	0.07	0.11	0.11	0.27	0.09

Table 8. Comparison of the strength estimated by FEA with the predicted design strength for long columns at elevated temperatures.

	Parameters	P_{FEA}/P_{EC}	$P_{FEA}/P_{EC,mod}$	P_{FEA}/P_{AISC}	$P_{FEA}/P_{AISC,mod}$	P_{FEA}/P_{DSM}	$P_{FEA}/P_{DSM,mod}$
Box section	Mean	1.31	1.12	1.43	1.11	1.09	1.09
	COV	0.08	0.06	0.18	0.07	0.06	0.06
H-section	Mean	1.39	1.17	1.73	1.17	1.18	1.18
	COV	0.07	0.05	0.11	0.06	0.05	0.05